

Predicting Short-duration GRB Rates in the Advanced LIGO Volume

TZVETELINA A. DIMITROVA,¹ NATHANIEL R. BUTLER,¹ AND SRIHARI RAVI¹

¹*Earth and Space Exploration, Arizona State University, P.O. Box 871404, Tempe, AZ 85287-1404, USA*

ABSTRACT

Starting with models for the compact object merger event rate, the short-duration Gamma-ray Burst (sGRB) luminosity function, and the *Swift*/BAT detector, we calculate the observed *Swift* sGRB rate and its uncertainty. Our probabilistic sGRB world model reproduces the observed number distributions in redshift and flux for 123 *Swift*/BAT detected sGRBs and can be used to predict joint sGRB/LIGO detection rates. We discuss the dependence of the rate predictions on the model parameters and explore how they vary with increasing experimental sensitivity. In particular, the number of bursts in the LIGO volume depends strongly on the parameters that govern sGRB beaming. Our results suggest that nearby sGRBs should be observed to have broader jets on average ($\theta_{\text{jet}} \gtrsim 30$ degrees), as compared to the narrowly-beamed appearance of cosmological sGRBs due to detection selection effect driving observed jet angle. Assuming all sGRBs are due to compact object mergers, within a $D < 200$ Mpc aLIGO volume, we predict $0.18_{-0.08}^{+0.19}$ sGRB/GW associations all-sky per year for on-axis events at *Swift* sensitivities, increasing to $1.2_{-0.6}^{+1.9}$ with the inclusion of off-axis events. We explore the consistency of our model with GW170817/GRB 170817A in the context of structured jets. Predictions for future experiments are made.

1. INTRODUCTION

Knowledge of Gamma-Ray Bursts (GRBs) has greatly benefited from the dramatic success of the *Swift* satellite (Gehrels et al. 2005), capable of rapid localization and highly-sensitive multi-wavelength observations that have enabled unprecedented ground-based followup and a high-rate of GRB redshift determinations. However, there remains relatively few short-duration GRB (sGRB) events with redshift measurements, and relatively little is understood about the properties of these populations (for an overview, see; Berger 2014).

The probable origin of sGRBs from mergers between binary compact objects such as binary neutron stars (BNS) and neutron star black hole (NSBH) binaries make them promising gravitational wave (GW) electromagnetic (EM) counterparts capable of detection by advanced interferometers. Following the success of the Laser Interferometer Gravitational-Wave Observatory (LIGO) in detecting GW150914, interest spiked in the sGRB population. The advanced aLIGO-Virgo discovery of GW170817 – near-simultaneous with GRB 170817A detected by the *Fermi* GRB Monitor (GBM) and International Gamma-Ray Astrophysics Laboratory (Abbott et al. 2017a) – provides direct evidence for BNS mergers as sGRB progenitors.

Here we seek to determine whether and how the cosmological sGRB population is consistent with the source progenitor merger population constrained by LIGO. We

employ a sample of 123 sGRBs detected by the Burst Alert Telescope (BAT) onboard *Swift*, and we carefully treat the *Swift*/BAT detection threshold to account for the majority of cosmological sGRBs which are undetected. We assume a universal model for the merger event rate, along with parameterized luminosity functions and beaming distributions, in order to better understand the sGRB population. The derived probabilistic sGRB world model successfully reproduces the observed *Swift*/BAT number distributions in z and flux, and it allows for predictions of the joint GW/sGRB detection rates for both on- and off-axis sGRBs. While the GW signal does not depend on beaming, the inclusion of distributions to describe sGRB beaming – and the resulting number of events pointed toward the observer – are essential to establishing a rate correspondence.

To set the stage, we carry-out an initial, approximate calculation. *Swift* detects about 2 sGRBs per year within 1 Gpc, based on 7 sGRBs with measured redshift over 15.7 years and a 20% rate of redshift determination. This corresponds to a mean, all-sky rate density for cosmological sGRBs of 20 ± 6 Gpc⁻³ yr⁻¹. Two aLIGO BNS events in two years of observation (within 200 Mpc; The LIGO Scientific Collaboration et al. 2021) implies a rate of 125 Gpc⁻³ yr⁻¹, assuming constant density. Roughly then, we expect an all-sky, joint detection rate of 0.16 ± 0.05 per year.

Separating sGRBs from their progenitor path is difficult (e.g., Sarin et al. 2022), and we will consider a rate

arXiv:2303.06598v1 [astro-ph.HE] 12 Mar 2023

model including both BNS and NSBH mergers. Due to a large uncertainty in the underlying mass ratios, The LIGO Scientific Collaboration et al. (2021) estimates a possible rate of BNS events as large as $\approx 2000 \text{ Gpc}^{-3} \text{ yr}^{-1}$, which dominates among the progenitor channels. This provides some flexibility for the source sGRB rate to be $\gtrsim 100$ times the observed rate. Assuming that all sGRBs are due to compact object mergers, that factor will limit the extent to which the sGRB population – not all of which are above detection threshold – can be beamed. We estimate a detection fraction $\lesssim 25\%$ within 1 Gpc, constraining our fits to yield a mean $\theta_{\text{jet}} > 17$ degrees (Section 4.3, below). We find that the observed jet angle is driven by the detection selection effect, where bias favoring bright events at increasing redshift makes the cosmological population appear quite narrowly-beamed, whereas events within the aLIGO’s lower distance volume are predicted to allow a wider mean $\theta_{\text{jet}} \gtrsim 30$ degrees to be seen.

1.1. Previous Estimates

Prior estimates of the GW/sGRB joint detection rate span a large range. Partially, the variation is due to pre-LIGO estimates without the benefit of LIGO constraints. It is also due in large part to differing assumptions regarding the extent of sGRB beaming.

Guetta & Piran (2005) consider sGRB/BNS associations and the effect of time-delay until merger on the redshift distribution and luminosity function and find a local sGRB rate of $\sim 0.8 \text{ Gpc}^{-3} \text{ yr}^{-1}$. Liu & Yu (2019) find a local sGRB rate of $\sim 3 - 4 \text{ Gpc}^{-3} \text{ yr}^{-1}$. Guetta & Piran (2006) find a much higher rate of $\sim 8 - 30 \text{ Gpc}^{-3} \text{ yr}^{-1}$ from redshift and luminosity distributions constrained by the *Swift*/*HETE-II* sample. Guetta & Stella (2008) predict that a large fraction of detectable GW events will coincide with sGRBs. Nakar et al. (2006) find a higher local rate as well of $> 10 \text{ Gpc}^{-3} \text{ yr}^{-1}$. Coward et al. (2012) account for dominant detection biases to find an sGRB rate density of $\sim 8_{-3}^{+5} - 1100_{-470}^{+700} \text{ Gpc}^{-3} \text{ yr}^{-1}$ out to $z \approx 0.5$, assuming isotropic emission and correcting for beaming. Assuming that all BNS mergers produce an sGRB, Siellez et al. (2013) estimate a simultaneous BNS-GW observation rate of $0.11 - 4.2 \text{ yr}^{-1}$ with *Swift* and *Fermi*. Under the assumption that a notable fraction of BNS mergers result in an sGRB, Coward et al. (2012) find a lower and upper detection rate limit for a aLIGO-Virgo search of $1 - 180 \text{ yr}^{-1}$.

Other recent studies attempt to also constrain sGRB beaming and present rates using these assumptions. Ghirlanda et al. (2016) estimate an sGRB rate within the aLIGO volume of $0.007 - 0.03 \text{ yr}^{-1}$ with jet open-

ing angles between 3 and 6 degrees. Liu & Yu (2019) estimate a similar rate of *Swift* detectable sGRBs in the aLIGO horizon of 0.032 yr^{-1} . Sarin et al. (2022) find a BNS merger rate of $384_{-213}^{+431} \text{ Gpc}^{-3} \text{ yr}^{-1}$, with an average $\theta_{\text{jet}} \sim 15$ degrees of BNS produced sGRBs. They report that an estimated 40% of BNS mergers produce jets, and measure a fraction $0.02_{-0.01}^{+0.02}$ of BNS events and 0.01 ± 0.01 NSBH mergers to result in observable sGRBs. Jin et al. (2018) use $\theta_{\text{jet}} \sim 0.1$ rad and a local BNS rate density of $\sim 1109_{-657}^{+1432} \text{ Gpc}^{-3} \text{ yr}^{-1}$, which decreases to $\sim 162_{-83}^{+140} \text{ Gpc}^{-3} \text{ yr}^{-1}$ when excluding a narrowly beamed sGRB. They find that off-axis sGRB events enhance the GW/sGRB rate to a 10% association probability.

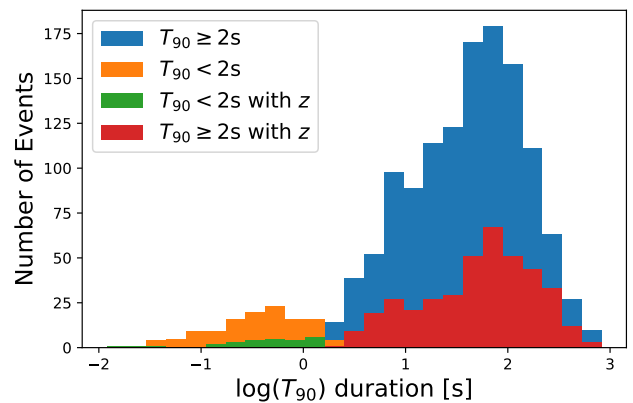


Figure 1. The separation of the GRB sample into short ($T_{90} < 2\text{s}$) and long-duration class, including events with and without measured z .

2. DATA RETRIEVAL AND SAMPLE SELECTION

We use publicly-available GRB data from the *Swift* BAT Gamma-Ray Burst Catalog¹ (Lien et al. 2016) for 1389 GRBs detected between December 17, 2004 and August 29, 2020. We retrieve burst duration intervals T_{90} , signal-to-noise ratios SNR , partial coding fractions f_p , redshifts z when available, and energy fluxes F (15-150 keV band). A detailed description of these quantities and relevant discussion may be found in the BAT catalog or in Butler et al. (2007). We apply a cutoff $T_{90} < 2\text{s}$ to define the short-duration burst population (e.g., Kouveliotou et al. 1993, ; also, Figure 1). To determine rest-frame luminosities, we assume a cosmology with $h = 0.71$, $\Omega_m = 0.3$, and $\Omega_\lambda = 0.7$. All error regions below correspond to the 90% confidence intervals, unless otherwise noted.

¹ <https://swift.gsfc.nasa.gov/results/batgrbcatalog>

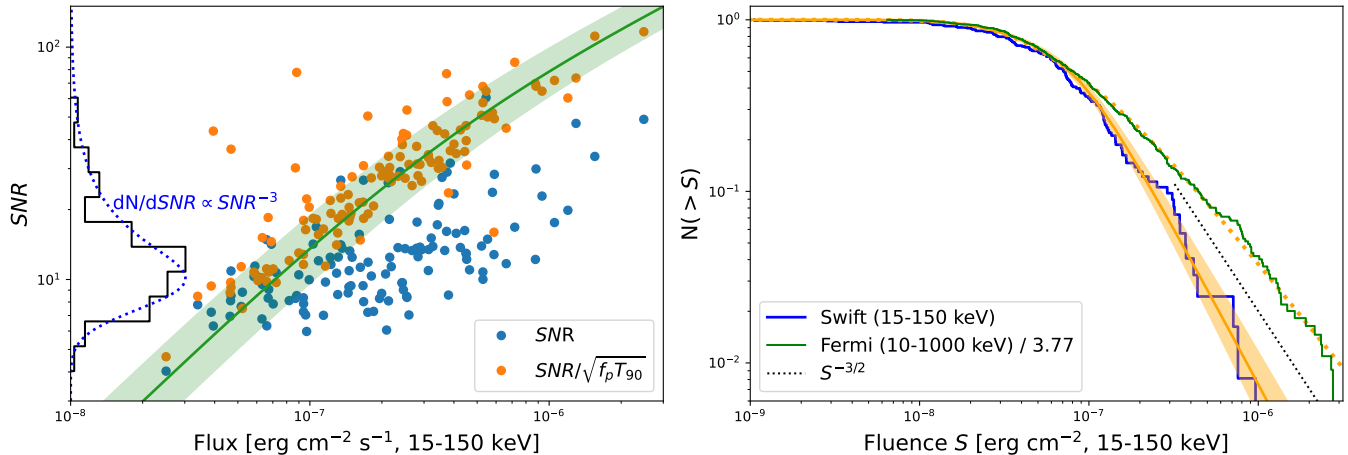


Figure 2. Left: Observed SNR values (blue points) – after correction to a fixed integration time and detector area (orange points) – correlate tightly with the observed 15-150 keV flux. The SNR histogram is shown with a fitted curve that yields a detection threshold in $\log(SNR)$ of 0.9 ± 0.1 (black; blue dashed). Right: The observed number of sGRBs over a range of Fluence S for *Swift* (15 – 150 keV band; blue) and *Fermi* (10 – 10³ keV band; green). The best-fit GRB world models for *Swift* (orange) and for *Fermi* (orange dashed) derived below are also plotted, including an $S^{0.5}$ bandpass correction factor for *Swift*.

A plot of the number of events versus a certain quantity can provide important lessons. The number of events with SNR above a given SNR , is quite steep, with a slope < -2 (Figure 2, Left). This may suggest a steep luminosity function, but it certainly indicates – as is well-known – that sGRBs tend to be weakly detected. The number of events with fluence (or flux) above a certain level, the so-called logN-logS relation, can be used to infer the nature of the source population. A logN-logS slope of $-3/2$ for a relatively nearby population (such as sGRBs) is only weekly-dependent upon the luminosity function and is indicative of a non-evolving source population (e.g., Longair 1966). Such a slope appears to be present at the bright end of the logN-logS relation (Figure 2, Right). The faint-end slope for sGRBs may also be near $-3/2$ after accounting for threshold effects (e.g., Petrosian & Lee 1996). However, to disentangle the physical effects that drive the number counts – to separately measure the luminosity function and the number density versus redshift – redshift measurements and a careful treatment of the detection limit are required. Parametric modelling is beneficial given the typically low SNR values.

In order to use the measured data to constrain intrinsic GRB properties, we need a prescription for mapping rest frame luminosities to observer frame fluxes and for deciding whether the observed fluxes are above the BAT detection threshold. We find that SNR for *Swift* can be predicted from the flux F with 0.1 dex scatter (i.e., 1σ spread; see, Figure 2, Left), as:

$$SNR = (F/F_0) \sqrt{T_{90} f_p} / \sqrt{2950 + F/F_0}. \quad (1)$$

Here, the zero point $F_0 = 1.2 \times 10^{-10}$ erg/cm²/s, and 2950 represents a typical background count rate. We note that the observed SNR distribution is very steep ($dN/dSNR \propto SNR^{-3}$) – indicating relatively little dynamic range in the sample – and is well-fit by a power-law truncated to zero at threshold and convolved with a Gaussian. This yields a stochastic SNR threshold of $10^{0.9 \pm 0.1}$.

We assume flux F and fluence S in the *Swift*/BAT bandpass are related as $S = FT_{90}$. Due to the low SNR values and the soft *Swift* bandpass, spectral parameters are typically poorly-constrained and the conversion to bolometric S is challenging. To simplify matters, we assume $S_{bol} = xS$, where x is a bandpass conversion factor applied to all bursts. We expect a large uncertainty of about a factor of 2 (0.3 dex) for x . We assume a mean correction $x = 3.77$ which is suitable for a typical, soft *Swift* sGRB spectrum ($E_{peak} \approx 250$ keV). A change to this value would alter the energetics scale (e.g., shift locations on some plots below).

This simple approach to a bolometric correction appears to break down for bright sGRBs (see, Figure 2, Right). In comparison with sGRB fluences from *Fermi*/GBM (Gruber et al. 2014; von Kienlin et al. 2014; Bhat et al. 2016; von Kienlin et al. 2020), we find that a larger correction is required for bright bursts. For bursts with $S > 10^{-7}$ erg/cm² (15-150 keV), we assume that the bolometric correction factor increases as $S^{0.5}$. This observer-frame effect likely arises due to the increasing hardness of bright bursts and the resulting lack of flux in the soft 15-150 keV band as compared to the harder, and approximately-bolometric 10-1000 keV

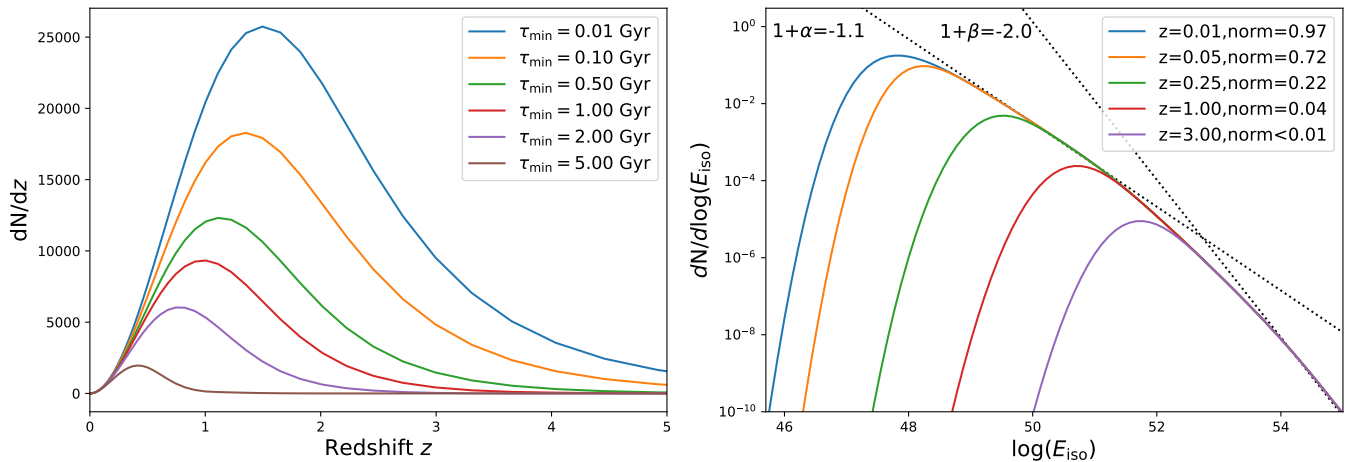


Figure 3. Left: Binary merger rates as a function of z from Safarzadeh et al. (2019) for different minimum time delays τ_{\min} between formation – which is assumed to track the SFR and Universal volume – and merger. Right: The E_{iso} luminosity function – found by integrating Equation 3 for the L_{γ} luminosity function over f_b – includes the detector threshold which increases with increasing z . The asymptotic power law behavior is shown with dotted lines. The integral of the model (see “norm” in legend) provides the fraction of sGRBs detected.

Fermi/GBM band. Although the effect is confirmed to correlate with hardness in the *Swift* 50-150 keV to 15-50 keV bands for 12 bursts measured in common between *Swift* and *Fermi*, we model it indirectly (on S alone) because a correction using the *Swift* hardness would introduce large errors and require spectral modelling not possible (with sufficient accuracy) given only the soft *Swift* bandpass. While a bandpass correction based on S only would not be an acceptable approach for individual burst modelling, it does capture the ensemble bandpass effects well. From Figure 2 (Right), we see that both *Swift* and *Fermi* have similar sGRB sensitivities (see also, Band 2003), and both have logN-logS distributions scaling roughly as $S^{-3/2}$ at the bright end.

Finally, we note that there are 3 events with anomalously high luminosities ($> 10^{52}$ erg/s) which we exclude from the analysis, but return to in Section 3.3 below. GRBs 090426 and 111117A have spectroscopic $z > 2$ and may lie on the short-duration end of the long-duration GRB population (see, Antonelli, L. A. et al. 2009; Levesque et al. 2010; Selsing, J. et al. 2018). GRB 120804A has an uncertain photometric $z = 1.3^{+0.3}_{-0.2}$ (1 sigma) based on a study of the host galaxy (Berger et al. 2013). Our final sample includes 123 sGRBs between and including GRB 050502 and GRB 20022A. Of these, 27 (22%) have measured redshifts in the catalog.

3. SGRB WORLD MODEL SUMMARY

Following Butler et al. (2010), to model the observed rates (number versus luminosity, number versus redshift z , number versus beaming fraction, etc.), we define functional forms for the probability distributions and, for a

given set of the parameters, use the intrinsic model to generate sGRBs reaching the detector. Not all of these will be detected, and evaluation of the extent to which the predicted rates from a given set of parameters match the observed rates requires the detector model above (e.g., Figure 2).

We assume a sGRB rate density model $\dot{\rho}(z)$ due to compact object mergers from Safarzadeh et al. (2019), which is a convolution of the star formation rate (SFR) and a merger delay time τ_d distribution. To convert from rate density to number N per redshift interval:

$$P_z(z) = \frac{dN}{dz} = \dot{\rho}(z) \frac{dV}{dz} \frac{1}{1+z}. \quad (2)$$

Here, V is the Universal volume at z , and the factor of $1+z$ converts rates at z to now. We assume a τ_d distribution $\propto \tau_d^{-1}$, where the maximum delay time is 10 Gyr and the minimum delay time (τ_{\min}) is a free-parameter. In principle, the -1 slope can also be varied; however this provides no additional model flexibility over the z range under study here. Resulting dN/dz distributions are shown in Figure 3 (Left). The rate density tracks the SFR for $\tau_{\min} \lesssim 100$ Myr and peaks at lower z for larger τ_{\min} .

The sGRB luminosity function is generally modelled as a single or broken power law, similar to studies of long-duration GRBs (see, e.g., Guetta & Piran 2006; Salvaterra et al. 2008; Virgili et al. 2011; D’Avanzo et al. 2014; Ghirlanda et al. 2016). To get the number of GRBs over a range of γ -ray Luminosity L_{γ} , we assume

$P_L = dN/dL_\gamma$, and

$$\begin{aligned} E_o \frac{dN}{dL_\gamma} &= A(L_\gamma/E_o)^\alpha, & E_{\min} < L_\gamma < E_o \\ &= A(L_\gamma/E_o)^\beta, & L_\gamma \geq E_o \end{aligned} \quad (3)$$

The luminosity function is defined above a minimum E_{\min} , allowing for it to be normalized (fixing A) assuming $\alpha \geq \beta$ and $\beta < -1$.

Choices for physical quantities to associate with L_γ include the total γ -ray energy reservoir, otherwise known as the beaming-corrected energy release E_γ , or the energy per solid angle as represented by the isotropic-equivalent energy release E_{iso} . Here, $E_\gamma = f_b E_{\text{iso}}$, for beaming fraction $f_b = 1 - \cos(\theta_{\text{jet}})$. Also, we are assuming the simple top-hat GRB jet model (e.g., Rhoads 1999; Frail et al. 2001), where the GRB is detected only if it launches a jet pointed in the direction of the observer. The rate of such events is proportional to the fraction of sky illuminated (i.e., f_b), establishing a direct relationship between outflow collimation and rates (see, also, Berger 2014).

To allow some flexibility between these possibilities, we write $L_\gamma = E_{\text{iso}} f_b^c$. The index c represents a potential correlation between f_b and E_γ . We allow c to vary between 0 and 1, allowing the luminosity argument to vary between E_{iso} ($c = 0$) and E_γ ($c = 1$). Viewed differently, the luminosity function is allowed to regulate GRBs in terms of total energetics ($c = 1$) or local properties ($c = 0$). We can motivate allowing this flexibility by noting that, during a GRB, the outside of the jet is not in causal contact with the inside of the jet; the processes that govern the observed GRB brightness distribution could depend weakly on the global energetics.

Since detection depends on E_{iso} , the observed f_b distribution will change with z for $c > 0$. With $c = 0$, the luminosity function depends on E_{iso} , and the observed f_b will take on an average value for all z . We assume a powerlaw $P_{f_b} = dN/df_b$ distribution (as in, e.g., Frail et al. 2001), with

$$dN/df_b = B f_b^n \quad (4)$$

The normalization B is set by integrating between a minimum $f_{b,\min} = 10^{-4}$ (corresponding to $\theta_{\text{jet},\min} = 0.8$ degrees) and a maximum $f_b = 1$. We apply a weak constraint on the beaming distribution:

$$n < -1.5 - c(1 + \alpha). \quad (5)$$

This prevents a flat, observed θ_{jet} distribution and corresponds to the statement ‘‘short-duration GRBs are beamed.’’

We assume a log-normal distribution of $\log(T_{90}) = -0.5 \pm 0.4$ and an exponential distribution for $\log(f_p)$ with mean -0.23 as in Butler et al. (2010).

Combining the above distributions, the predicted, observed event rate density r is:

$$\begin{aligned} r &= r_o f_b P_{f_b}(f_b|n) P_z(z|\tau_{\min}) P_L(L_\gamma|\alpha, \beta, c, E_{\min}, E_o) \\ &\quad \times H(L_\gamma - L_{\text{th}}) P_{th}(L_t|L_{\gamma,\min}). \end{aligned} \quad (6)$$

Here, $L_\gamma = 4\pi D_L^2/(1+z)xSf_b^c$, and the minimum detectable $L_{\gamma,\min} = 4\pi D_L^2/(1+z)xS_{\min}(T_{90}, f_p)f_b^c$, and H is the Heaviside step function. The threshold L_{th} distribution $P_{th}(L_{\text{th}})$ is assumed to be log-normal with a mean of $L_{\gamma,\min}$ and a standard deviation of 0.35 dex. This accounts for the uncertain conversions from limiting SNR to limiting *Swift* 15–350 keV S (0.14–0.18 dex, depending on whether we fix T_{90} and f_b or average over the observed values) and then from *Swift* S to bolometric S (0.3 dex). The contribution to the scatter from averaging over T_{90} and f_p is negligible, and we can effectively marginalize over those distributions when calculating the distribution normalization by assuming their mean values.

3.1. Model Normalization

We assume all sGRBs are due to compact object mergers. The normalization r_o in Equation 6 includes 3 factors, 1 fixed and 2 variable which become model parameters requiring priors. First is the fixed $\Omega/(4\pi)$ fraction of sky covered by *Swift*, for which we assume $\Omega = 1.3$ str, multiplied by a *Swift* observation period of 15.7 years. Second is the rate of merger events in the $D < 200$ Mpc aLIGO volume. This normalization factor is represented by a gamma function prior corresponding to 2 BNS events (GW170817 and GW190425, Abbott et al. 2017b; Abbott et al. 2020) detected in 2 years (O1 through O3). Third is a factor that scales the $D < 200$ Mpc yearly rate out to a $D = 1$ Gpc yearly rate appropriate for sGRBs. The third normalization factor is highly-uncertain based on LIGO team estimates (The LIGO Scientific Collaboration et al. 2021) and is assumed to be distributed uniformly between 1 and 10. We choose a distance of 200 Mpc as a representative LIGO sensitivity volume for BNS events; LIGO is expected to detect BNS events out to 190 Mpc in the O4 observing run (2023–2024) and out to 325 Mpc in O5 (2026–2028)².

3.2. The Distribution of E_{iso} , given z

² <https://observing.docs.ligo.org/plan>

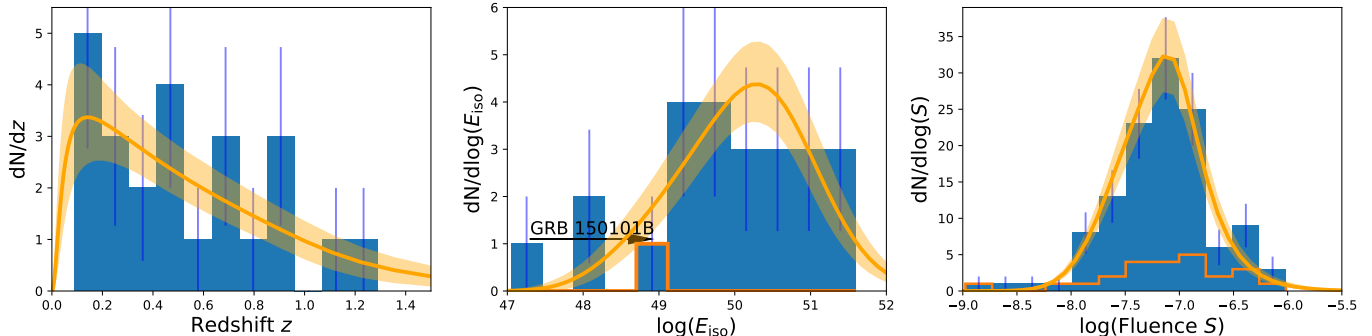


Figure 4. The observed (blue) and predicted (orange) rates of sGRBs with respect to z (Left), E_{iso} (Middle), and S (Right). The right panel includes all sGRBs in the blue histogram and also displays the sGRBs with measured z as a superimposed, unshaded orange histogram. GRB 150101B is discussed in Section 4.1.

To fit the data, we require P_E : the distribution of E_{iso} , given z . We construct P_E by multiplying the luminosity function by the beaming distribution, and the detection distributions by f_b , evaluating at $L_\gamma = f_b^c E_{\text{iso}}$, and integrating over f_b . The integration over f_b results in a smoothly-broken powerlaw with low-energy slope α and high-energy slope β (see, Figure 3; Right). The transition between slopes occurs over an extended range in E_{iso} from E_o until E_o/f_b^c . To be explicit, starting from Equation 6:

$$r = r_o P_z(z|\tau_{\text{min}}) P_E(E_{\text{iso}}|z, n, \alpha, \beta, c, E_{\text{min}}, E_o), \quad (7)$$

with

$$P_E = \int f_b P_{f_b} P_L(E_{\text{iso}} f_b^c) H(E_{\text{iso}} f_b^c - L_{\text{thresh}}) P_t df_b. \quad (8)$$

We first calculate P_E analytically at $z = 0$ (i.e., all events detected), and ensure that it is normalized. The detection distributions HP_t are then applied as a z -dependent cutoff at $L_{\text{thresh}} = E_{\text{iso}} f_b^c$, followed by a Gaussian convolution to get the observed distribution in E_{iso} at a given z .

From P_E and P_z , it is then possible to calculate the joint distribution of S and z and the marginal distributions for E_{iso} , S , or z . The integrations over E_{iso} , S , and z are carried out numerically over fine grids, with the z grid extending from $z = 7.1 \times 10^{-4}$ (i.e., $D = 3$ Mpc) to $z = 10$. Figure 3 (Right) displays the E_{iso} luminosity function at different z values.

3.3. Model Fitting

In fitting the above models by matching the model and observed rates, we treat the measured values of z , T_{90} , f_p , and S (and E_{iso} fixed by z and S) as point estimates only (i.e., having no error). The uncertainty in these quantities is placed in the models, which can be considered smoothed to avoid over-fitting.

The parameters $\vec{\theta}$ are n , c , E_{min} , α , β , E_o , and τ_{min} . The observables \vec{D} are z , S , T_{90} , and f_p . The rate evaluated for a given event i is written r_i . In the case of GRBs with no measured z , we integrate r_i over z . To find the parameters that best fit the model, we maximize the Poisson likelihood:

$$\mathcal{L}(\vec{D}|\vec{\theta}) = \exp \left[- \int r d\vec{D} \right] \prod_{i=1}^N r_i(\vec{\theta}) \quad (9)$$

The integral in the exponential in Equation 9, with $d\vec{D} = dz dS dT_{90} df_p$, yields the total number of predicted events. Prior to crawling the parameter space $\vec{\theta}$ via Markov Chain Monte Carlo (MCMC) maximization of $\log(\mathcal{L})$, we first marginalize analytically over r_o (see, Equation 7).

The MCMC analysis is carried out with PyMC3 (Salvatier et al. 2016), using multiple chains at a variety of starting parameter values to establish uniqueness of the derived solution. We assume uniform prior distributions on all parameters except for E_{min} and E_o . Also included are the luminosity function slope constraints (Section 3) and constraints on the f_b distribution (Equation 5). For E_{min} and E_o we assume log-normal priors, $\log(E_{\text{min}}) = 47.8 \pm 0.5$ and $\log(E_o) = 50.5 \pm 0.3$. The $\log(E_{\text{min}})$ prior is weak and non-constraining. The tighter E_o prior is designed to test for the possibility of a break in the luminosity function.

The posterior parameter distributions are estimated by drawing 10^4 parameter $\vec{\theta}$ samples from the MCMC, after thinning by a factor of 4 to limit draw-to-draw correlations. These are summarized in Table 1 and discussed more in Section 4.3 below. We generate posterior distributions for the observables \vec{D} by averaging their distributions from Section 3.2 over the sampled parameters.

4. DISCUSSION

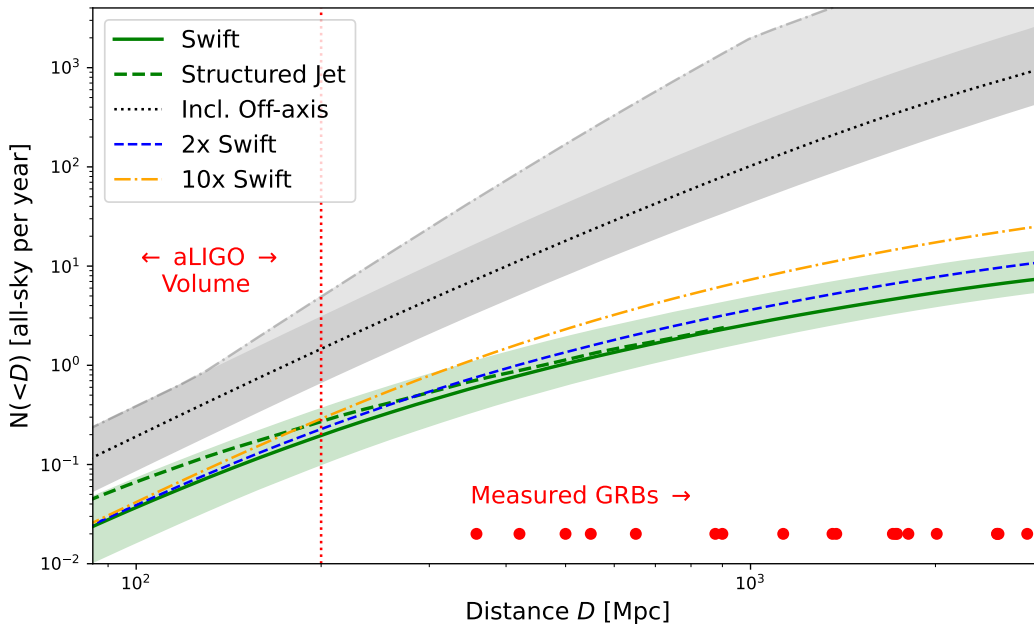


Figure 5. The all-sky predicted number of sGRBs per year as a function of distance, detectable by *Swift*. On-axis events are displayed in green, and on- and off-axis bursts are displayed in black. Increased detector area (blue and orange curves) strongly-affect the predicted rate at $D \gtrsim 1$ Gpc. Structured jets (dashed green curve) are discussed in Section 5.

Table 1. MCMC Parameters 90% Confidence Intervals

Parameter	Value (all GRBs)
f_b index n	-0.7 ± 0.3
correlation index c	> 0.6
$\log(E_{\min})$	47.3 ± 0.4
α	-2.1 ± 0.2
β	$-2.5^{+0.3}_{-2.1}$
$\log(E_o)$	$50.5^{+0.6}_{-0.3}$
τ_{\min}	< 700 Myr

4.1. Predicted Observable Distributions

Predicted distributions and uncertainties for z , E_{iso} , and S are overplotted on the observed data in Figure 4. The models fit the observed data well. The best-fit fluence model (Figure 4; Right), for example, has a reduced $\chi^2_\nu = 1.1$ for $\nu = 4$ degrees of freedom, using the Gehrels (1986) approximate for the standard deviation of Poisson counts.

While the observed redshift distribution peaks at $z \approx 0.2$, this is largely due to the decline in detection efficiency at high- z (Figure 3; Right). The input redshift distribution – Equation 2 averaged over draws of the τ_{\min} parameter – peaks at $z = 1.35$, as compared to $z = 1.45$ for the SFR. We estimate a modest, 73% confidence that the rate model is delayed with respect to

the SFR by counting the fraction of draws with a peak below $z = 1.4$.

The predicted distributions for E_{iso} and fluence S are also closely consistent with the data. However, we note that in the middle panel of Figure 4, there is a possible outlier. GRB 150101B was an un-triggered event also detected by *Fermi*/GBM with a significantly higher reported flux (leading to $E_{\text{iso}} = 1.1 \times 10^{49}$ erg instead of 1.6×10^{47} erg (Burns et al. 2018). GRB 150101B may have also been an off-axis event (Troja et al. 2018).

In the fitting above, we have assumed that events with z should be fit alongside events without redshift. This can be justified by the similarity of the observed S distributions in Figure 4 (Right). From a two-sample Kolmogorov-Smirnov test, we find that the distributions cannot be significantly differentiated ($\tau = 0.168$; p-value 0.58).

The evidence for a break in the luminosity function is formally strong (99% confidence), given the confidence intervals for α and β . However, the measurement of E_o without the restrictive prior is highly uncertain given the smooth shape of the luminosity function that results from the uncertainty in our E_{iso} measurements and the additional smoothing caused by integration over f_b . Moreover, it is important to note that the possible measurement of a break depends on the sample selec-

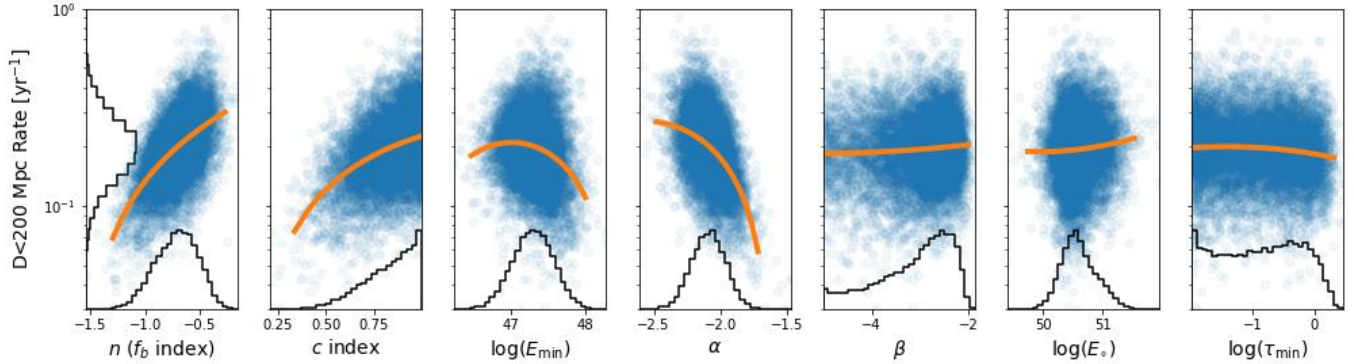


Figure 6. The number of on-axis sGRBs expected within the aLIGO volume, displayed versus the different parameters. Quadratic curves are plotted through the parameter samples to highlight possible trends. Overall distributions are displayed as histograms on both axes (see also, Table 1).

tion. If we include the 3 high-luminosity events in our fitting (GRBs 090426, 111117A, and 120804A; Section 2), the slopes become entirely consistent ($\alpha = -2.1^{+0.2}_{-0.1}$, $\beta = -2.2 \pm 0.1$) with a single power-law luminosity function. Also, including these events lowers the upper limit on τ_{\min} (30 versus 700 Myr). The other model parameters in Table 1 are not significantly altered.

4.2. GRB Rate Predictions

The integral of Equation 8 over E_{iso} at a given z , averaged over MCMC parameters (Table 1), provides the total, predicted event rate for on-axis sGRBs as a function of redshift. If we omit the first f_b factor from the integral, we can determine the predicted event rate for all sGRBs on- or off-axis as a function of redshift. These curves and their uncertainties given the spread in model parameters are displayed in Figure 5. The curves are generated assuming the *Swift* sensitivity but all-sky coverage.

At large distances ($D \gtrsim 1$ Gpc), the satellite sensitivity becomes important as many events are lost below threshold. Curves for hypothetical satellites with sensitivities two times and ten times greater than *Swift* are displayed. For distances below 1 Gpc and above 200 Mpc, the dominant rate uncertainty is due to the uncertainty in the total number of BNS mergers as constrained by LIGO (The LIGO Scientific Collaboration et al. 2021). This uncertainty is displayed using a dot-dashed curve at the top of Figure 5.

Below 200 Mpc, essentially all sGRBs are detected by *Swift* according to our modelling. The number of events detectable all-sky per year at *Swift* sensitivities within the aLIGO volume is $0.18^{+0.19}_{-0.08}$ for on-axis events – in agreement with our rough calculation in Section 1 – and increases to $1.2^{+1.9}_{-0.6}$ with the inclusion of off-axis events.

4.3. Rate Dependence on Beaming, Other Parameters

In Figure 6, we display the predicted rate determined for each parameter draw, with a separate sub-panel dedicated to each parameter. A quadratic curve is fit in each sub-panel to highlight trends. Significant trends are observed for 3 parameters: n , c , and α .

When the low-energy powerlaw index for the luminosity function α is steep, there is naturally an increased rate of faint, nearby events. This effect can be observed weakly in the E_{\min} parameter as well. However, the impact of that parameter is limited by the fact that E_{\min} values below the observed range of measured E_{iso} values would lead to an over-large model normalization and be penalized by the exponential term in Equation 9.

Several of the parameters are correlated with each other as a result of the flux limit and the beaming constraint Equation 5. The rate-density parameter, however, is uncorrelated with the other parameters, except for a weak correlation with α for long delay times ($\tau_{\min} > 500$ Myr).

We note that our derived luminosity function slopes $\alpha \approx -2$ are considerably steeper than $\alpha \approx -0.5$ found in Ghirlanda et al. (2016). While we do not claim strong evidence for a break in the luminosity function (Section 4.1), and therefore a clean separation between the slopes α and β , we do find that the overall luminosity function is steep.

The steeper luminosity function likely arises from our approach to the modelling of beaming. A large, negative value for n corresponds to a highly-beamed population where the bulk of sGRBs are pointed away from the observer. It is not possible to generate the observed sGRB population from compact object mergers if n is too negative. However, with f_b present in the luminosity function, an interesting effect arises where a steep $\alpha < -1$ permits a larger n (i.e., more GRBs pointed at the observer; see, Equation 5).

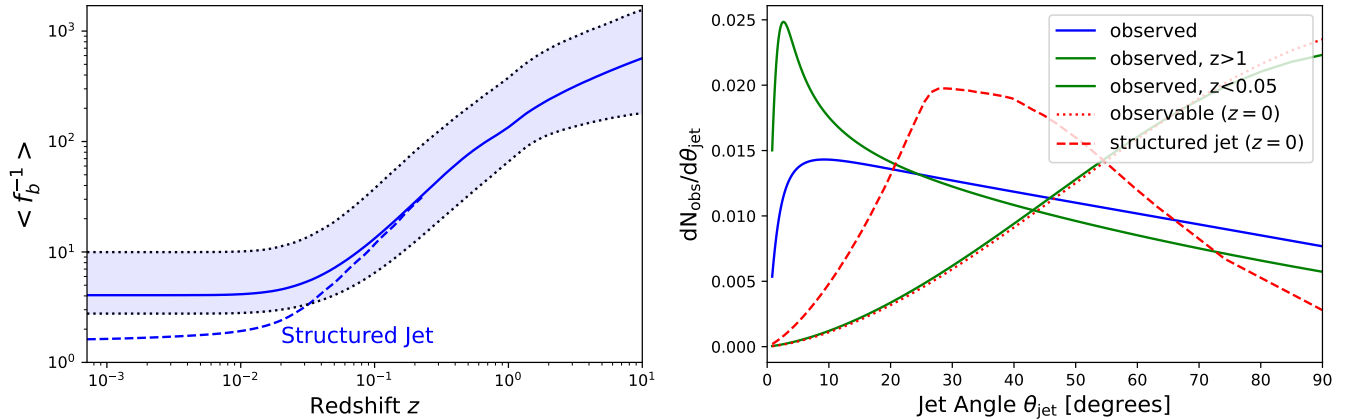


Figure 7. Left: Mean inverse beaming fraction $\langle f_b^{-1} \rangle$ – proportional to the number of missed events – and confidence intervals (dotted lines, blue shaded regions) of sGRBs as a function of z . Right: The mean distribution of sGRB jet angles $dN_{\text{obs}}/d\theta_{\text{jet}}$. We show the predicted observed (blue, $z > 1$ green) distributions as well as those expected for an ideal instrument (i.e., $z = 0$; red dotted). Structured jets (dashed curves) are discussed in Section 5.

The effect of a correlation index c near unity is to make the luminosity function depend on E_γ . The data prefer a luminosity function depending on E_γ rather than E_{iso} ($c > 0.5$ at 98% confidence). In this case, there arises a significant detection bias in favor of narrowly-beamed events with increasing redshift (see, Figure 7). The observed cosmological sGRB population (i.e., at high- z) appears narrowly beamed (satisfying the constraint Equation 5), while the low- z population tends to be more broadly beamed, leading to a higher predicted rate.

Direct constraints on sGRB jet opening angles from afterglow jet-break measurements are rare. Fong (2014) present a complete tabulation of sGRB beaming angles measurements and limits available prior to 2014. From 4 measurements of jets with $\theta_{\text{jet}} \approx 5$ degrees and 9 upper limits (as large as 25 degrees), Berger (2014) estimate a mean $\theta_{\text{jet}} > 10$ degrees. Our predictions are consistent with these constraints (see, Figure 7; Right), allowing for large beaming angles but implying that the cosmological population should appear significantly more tightly beamed than the general population. We find a most-likely $\theta_{\text{jet}} = 2.6$ degrees for $z > 1$ as compared to $\theta_{\text{jet}} = 9$ degrees for all z .

An additional important model parameter not displayed in Figure 6 is the normalization. To reproduce all cosmological sGRBs we must exploit the large (factor of 10) uncertainty in the BNS rate within 1 Gpc (Sections 1, 3.1). We find that this factor must be > 5 (90% confidence), corresponding to a BNS rate $> 10^3$ Gpc $^{-3}$.

5. CONCLUSIONS

We have demonstrated that a sample of 123 sGRBs from *Swift* – including 27 events with measured red-

shifts – can be generated from the source aLIGO merger population, in turn deriving probabilistic estimates for the sGRB rate density, the luminosity function, and the beaming distribution. The rate-density appears to allow for a range of merger delay times ($\tau_{\text{d,min}} < 700$ Myr) and suggests contributions from BNS and NSBH progenitor channels (e.g., Safarzadeh et al. 2019; Sarin et al. 2022), although we have not attempted to disentangle these contributions. The luminosity function is a relatively steep ($\alpha \approx -2$), possibly-broken powerlaw operating on E_{iso} and the beaming fraction f_b and leading to a correlation between the two. As a result, we predict relatively wide sGRB jet angles, particularly for nearby events.

We predict $0.18_{-0.08}^{+0.19}$ GW/sGRB associations per year, all-sky, for on-axis events at *Swift* sensitivities within the $D < 200$ Mpc aLIGO volume. This increases to $1.2_{-0.6}^{+1.9}$ yr $^{-1}$ with the inclusion of off-axis events. These very nearby events have a broad, jet-opening angle distribution, with mean $\theta_{\text{jet}} \gtrsim 30$ degrees, while cosmological sGRBs above the detection limit appear to have narrower jet opening angles as a result of a correlation between E_{iso} and the beaming factor (e.g., Figure 7).

In the context of our sGRB world model (Section 3), it is interesting to explore the uniqueness of GRB 170817A, associated with GW170817 (Abbott et al. 2017). The *Fermi*/GBM fluence – measured over the T_{90} duration interval – for GRB 170817A was 2.8×10^{-7} erg cm $^{-2}$ (10-1000 keV; Goldstein et al. 2017). The corresponding $E_{\text{iso}} = 5.35 \times 10^{46}$ erg. In our model (see, Figure 8), such a low E_{iso} would be associated with a spherical, or nearly spherical explosion. However, GRB 170817A was an exceptionally off-axis event, with an X-ray afterglow that peaked 160 days after the

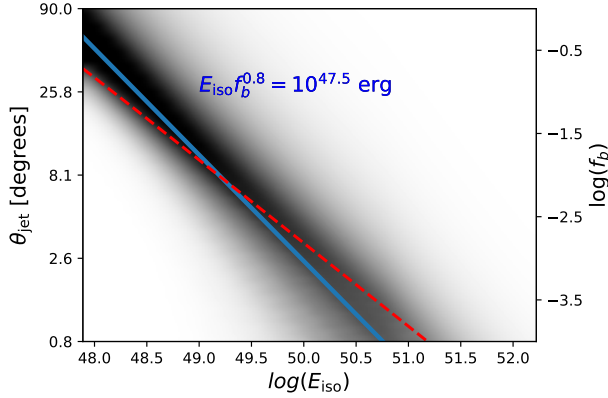


Figure 8. The joint E_{iso}, f_b distribution at $z = 0$. The correlation between E_{iso} and f_b appears as a broad ridge around $E_{\text{iso}} f_b^c = 10^{47.5}$ (solid blue curve) erg as a consequence of the steep luminosity function with a minimum energy (Section 4.1). The similar curve corresponding to a “standard” sGRB E_γ ($E_{\text{iso}} \propto \theta_{\text{jet}}^2$) using the small-angle formula is shown for reference (dashed red curve).

sGRB (Troja et al. 2020). Although the on-axis energetics remain unconstrained, it is likely that the GRB was viewed at an angle $\theta_{\text{view}} \sim 5\theta_{\text{jet}}$ (see, Nakar & Piran 2021, and references therein). In our model, a broadly-jetted $\theta_{\text{jet}} = 15$ degree and $E_{\text{iso}} = 10^{49}$ erg event is 10^2 – 10^3 times more likely than a $\theta_{\text{jet}} = 5$ degree event with energies comparable to those of the brightest, cosmological sGRBs ($E_{\text{iso}} \approx 10^{51}$ – 10^{52} erg; Figure 4).

Although the off-axis nature of GRB 1701817A is clearly an important clue as to the GW association, it does not suggest that we should increase our on-axis rate predictions significantly toward our (larger) on- and off-axis rate predictions (Figure 5). In the flat-top jet model (e.g., Ioka & Nakamura 2017) or structured jet models (e.g., Nakar & Piran 2021), the on-axis event could be very bright ($E_{\text{iso}} \gtrsim 10^{52}$ erg), hence highly-unusual at such a nearby distance of 40 Mpc. Similarly, if $E_{\text{iso}} = 5.35 \times 10^{46}$ erg is instead taken to be typical of the nearly-spherical emission that may accompany sGRBs, it is only detectable at distances $D \lesssim 60$ Mpc by *Swift* or *Fermi*, leading to a predicted rate increase of only 16% in a 200 Mpc aLIGO volume.

A Gaussian structured jet model can increase the observable solid angle significantly for nearby events (by a factor of 1.4 for $D < 200$ Mpc, and 2.2 for $D < 40$ Mpc; Figure 5; see, also Howell et al. 2019). Here, instead of $f_b = 1 - \cos(\theta_{\text{jet}})$, we write:

$$f_b = \int \exp(-(\theta/\theta_o)^2) \sin(\theta) d\theta. \quad (10)$$

To capture the same asymptotic behavior for small θ_{jet} and $\theta_{\text{jet}} = 90$ degrees, we set $\theta_o = \tan(\theta_{\text{jet}})$. Equation 10 does not change the above analysis for cosmological GRBs which sample only the core of the jet; however the observable angles – for nearby and narrowly-jetted events where the minimum-detectable $E_{\text{iso},\text{min}} < E_{\text{min}}/f_b^c$ – can be significantly wider than θ_{jet} . This is because the first factor of f_b in Equation 6 is replaced with $1 - \cos(\theta_{\text{view}})$, where $\theta_{\text{view}}^2 = \theta_o^2 \ln(L_\gamma/L_{\gamma,\text{min}})$. This also tends to favor narrowly-jetted events. For $D < 40$ Mpc, the most likely $\theta_{\text{jet}} = 29$ degrees (see, Figure 7) and the mean viewing angle is $\theta_{\text{view}} \approx 60$ degrees.

The resulting sGRB flux is near the detection threshold. It is possible that such events could be identified, likely in a non-decisive manner, after an optical counterpart is found and the number of search trials is reduced.

Predicted on-axis sGRBs within the aLIGO volume, however, are well-above (factor of 26 on average) the *Swift*/BAT threshold. We estimate that the majority would be detected even using a down-scaled instrument with 80 times smaller effective area. More important than sensitivity, *Swift* itself can be expected to detect very few associations (0.018 yr^{-1} per 1.3 sr) due to its narrow field of view. Experiments with large fields of view, like *Fermi*/GBM (0.09 yr^{-1} per 2π sr), are far more likely to be successful. To the extent that GRB 170817A is in any way typical, and off-axis emission is generally-detectable, a sensitive and wide-field experiment like *Fermi*/GBM is optimal (approaching 0.6 yr^{-1} per 2π sr).

Nonetheless, our estimates are fundamentally-limited by a scarcity of constraints on sGRB beaming. Additional sGRB detections and followup – including deep followup with Rubin Observatory (Ivezic et al. 2019) to measure or limit the orphan afterglow (Rhoads 1999) rate – is needed to better constrain sGRB jetting and to further probe the relation between sGRBs and GW events.

Similarly, future GW detections in O4 and O5 with increasing sensitivity (e.g., Williams et al. 2018), can further constrain the BNS rate beyond 200 Mpc and place more challenging constraints on sGRB beaming. Under the uncertainty in the fraction of GW events that result in jetting (The LIGO Scientific Collaboration et al. 2021), reproducing the GRB rate from the GW rate will be a greater challenge if not all GW events can produce a jet. If future GW observations constrain the BNS rate to $\lesssim 1 \text{ Gpc}^{-1}$ (see, Section 4.3), our starting assumption that all – or even most – sGRBs are due to compact object mergers is likely incorrect.

REFERENCES

- Abbott, B. P., Abbott, R., Abbott, T. D., et al. 2017a, *The Astrophysical Journal*, 848, L13, doi: [10.3847/2041-8213/aa920c](https://doi.org/10.3847/2041-8213/aa920c)
- . 2017b, *Phys. Rev. Lett.*, 119, 161101, doi: [10.1103/PhysRevLett.119.161101](https://doi.org/10.1103/PhysRevLett.119.161101)
- Abbott, B. P., Abbott, R., Abbott, T. D., et al. 2017, *ApJL*, 848, L12, doi: [10.3847/2041-8213/aa91c9](https://doi.org/10.3847/2041-8213/aa91c9)
- . 2020, *ApJL*, 892, L3, doi: [10.3847/2041-8213/ab75f5](https://doi.org/10.3847/2041-8213/ab75f5)
- Antonelli, L. A., D’Avanzo, P., Perna, R., et al. 2009, *A&A*, 507, L45, doi: [10.1051/0004-6361/200913062](https://doi.org/10.1051/0004-6361/200913062)
- Band, D. L. 2003, *ApJ*, 588, 945, doi: [10.1086/374242](https://doi.org/10.1086/374242)
- Berger, E. 2014, *Annual Review of Astronomy and Astrophysics*, 52, 43, doi: [10.1146/annurev-astro-081913-035926](https://doi.org/10.1146/annurev-astro-081913-035926)
- Berger, E., Zauderer, B. A., Levan, A., et al. 2013, *The Astrophysical Journal*, 765, 121, doi: [10.1088/0004-637x/765/2/121](https://doi.org/10.1088/0004-637x/765/2/121)
- Bhat, P. N., Meegan, C. A., von Kienlin, A., et al. 2016, *The Astrophysical Journal Supplement Series*, 223, 28, doi: [10.3847/0067-0049/223/2/28](https://doi.org/10.3847/0067-0049/223/2/28)
- Burns, E., Veres, P., Connaughton, V., et al. 2018, *The Astrophysical Journal*, 863, L34, doi: [10.3847/2041-8213/aad813](https://doi.org/10.3847/2041-8213/aad813)
- Butler, N. R., Bloom, J. S., & Poznanski, D. 2010, *The Astrophysical Journal*, 711, 495, doi: [10.1088/0004-637X/711/1/495](https://doi.org/10.1088/0004-637X/711/1/495)
- Butler, N. R., Kocevski, D., Bloom, J. S., & Curtis, J. L. 2007, *The Astrophysical Journal*, 671, 656, doi: [10.1086/522492](https://doi.org/10.1086/522492)
- Coward, D. M., Howell, E. J., Piran, T., et al. 2012, *Monthly Notices of the Royal Astronomical Society*, 425, 2668, doi: [10.1111/j.1365-2966.2012.21604.x](https://doi.org/10.1111/j.1365-2966.2012.21604.x)
- D’Avanzo, P., Salvaterra, R., Bernardini, M. G., et al. 2014, *MNRAS*, 442, 2342, doi: [10.1093/mnras/stu994](https://doi.org/10.1093/mnras/stu994)
- Fong, W.-f. 2014, PhD thesis, Harvard Smithsonian Center for Astrophysics
- Frail, D. A., Kulkarni, S. R., Sari, R., et al. 2001, *ApJL*, 562, L55, doi: [10.1086/338119](https://doi.org/10.1086/338119)
- Gehrels, N. 1986, *ApJ*, 303, 336, doi: [10.1086/164079](https://doi.org/10.1086/164079)
- Gehrels, N., Chincarini, G., Giommi, P., et al. 2005, *The Astrophysical Journal*, 621, 558, doi: [10.1086/427409](https://doi.org/10.1086/427409)
- Ghirlanda, G., Salafia, O. S., Pescalli, A., et al. 2016, *A&A*, 594, A84, doi: [10.1051/0004-6361/201628993](https://doi.org/10.1051/0004-6361/201628993)
- Goldstein, A., Veres, P., Burns, E., et al. 2017, *ApJL*, 848, L14, doi: [10.3847/2041-8213/aa8f41](https://doi.org/10.3847/2041-8213/aa8f41)
- Gruber, D., Goldstein, A., von Ahlefeld, V. W., et al. 2014, *The Astrophysical Journal Supplement Series*, 211, 12, doi: [10.1088/0067-0049/211/1/12](https://doi.org/10.1088/0067-0049/211/1/12)
- Guetta, D., & Piran, T. 2005, *A&A*, 435, 421, doi: [10.1051/0004-6361:20041702](https://doi.org/10.1051/0004-6361:20041702)
- . 2006, *A&A*, 453, 823, doi: [10.1051/0004-6361:20054498](https://doi.org/10.1051/0004-6361:20054498)
- Guetta, D., & Stella, L. 2008, *Astronomy & Astrophysics*, 498, 329, doi: [10.1051/0004-6361:200810493](https://doi.org/10.1051/0004-6361:200810493)
- Howell, E. J., Ackley, K., Rowlinson, A., & Coward, D. 2019, *Monthly Notices of the Royal Astronomical Society*, 485, 1435, doi: [10.1093/mnras/stz455](https://doi.org/10.1093/mnras/stz455)
- Ioka, K., & Nakamura, T. 2017, *Progress of Theoretical and Experimental Physics*, 2018, doi: [10.1093/ptep/pty036](https://doi.org/10.1093/ptep/pty036)
- Ivezić, Ž., Kahn, S. M., Tyson, J. A., et al. 2019, *ApJ*, 873, 111, doi: [10.3847/1538-4357/ab042c](https://doi.org/10.3847/1538-4357/ab042c)
- Jin, Z.-P., Li, X., Wang, H., et al. 2018, *ApJ*, 857, 128, doi: [10.3847/1538-4357/aab76d](https://doi.org/10.3847/1538-4357/aab76d)
- Kouveliotou, C., Meegan, C. A., Fishman, G. J., et al. 1993, *ApJL*, 413, L101, doi: [10.1086/186969](https://doi.org/10.1086/186969)
- Levesque, E. M., Bloom, J. S., Butler, N. R., et al. 2010, *Monthly Notices of the Royal Astronomical Society*, 401, 963, doi: [10.1111/j.1365-2966.2009.15733.x](https://doi.org/10.1111/j.1365-2966.2009.15733.x)
- Lien, A., Sakamoto, T., Barthelmy, S. D., et al. 2016, *The Astrophysical Journal*, 829, 7, doi: [10.3847/0004-637X/829/1/7](https://doi.org/10.3847/0004-637X/829/1/7)
- Liu, H.-Y., & Yu, Y.-W. 2019, *Research in Astronomy and Astrophysics*, 19, 118, doi: [10.1088/1674-4527/19/8/118](https://doi.org/10.1088/1674-4527/19/8/118)
- Longair, M. S. 1966, *MNRAS*, 133, 421, doi: [10.1093/mnras/133.4.421](https://doi.org/10.1093/mnras/133.4.421)
- Nakar, E., Gal-Yam, A., & Fox, D. B. 2006, *ApJ*, 650, 281, doi: [10.1086/505855](https://doi.org/10.1086/505855)
- Nakar, E., & Piran, T. 2021, *ApJ*, 909, 114, doi: [10.3847/1538-4357/abd6cd](https://doi.org/10.3847/1538-4357/abd6cd)
- Petrosian, V., & Lee, T. T. 1996, in *American Institute of Physics Conference Series*, Vol. 366, High Velocity Neutron Stars, ed. R. E. Rothschild & R. E. Lingenfelter, 170–174
- Rhoads, J. E. 1999, *ApJ*, 525, 737, doi: [10.1086/307907](https://doi.org/10.1086/307907)
- Safarzadeh, M., Berger, E., Ng, K. K. Y., et al. 2019, *The Astrophysical Journal*, 878, L13, doi: [10.3847/2041-8213/ab22be](https://doi.org/10.3847/2041-8213/ab22be)
- Salvaterra, R., Cerutti, A., Chincarini, G., et al. 2008, *MNRAS*, 388, L6, doi: [10.1111/j.1745-3933.2008.00488.x](https://doi.org/10.1111/j.1745-3933.2008.00488.x)
- Salvatier, J., Wiecki, T. V., & Fonnesbeck, C. 2016, *PeerJ Computer Science*, 2, e55
- Sarin, N., Lasky, P. D., Vivanco, F. H., et al. 2022, *PhRvD*, 105, 083004, doi: [10.1103/PhysRevD.105.083004](https://doi.org/10.1103/PhysRevD.105.083004)
- Selsing, J., Krühler, T., Malesani, D., et al. 2018, *A&A*, 616, A48, doi: [10.1051/0004-6361/201731475](https://doi.org/10.1051/0004-6361/201731475)
- Siellez, K., Boër, M., & Gendre, B. 2013, *Monthly Notices of the Royal Astronomical Society*, 437, 649, doi: [10.1093/mnras/stt1915](https://doi.org/10.1093/mnras/stt1915)

- The LIGO Scientific Collaboration, the Virgo Collaboration, the KAGRA Collaboration, et al. 2021, arXiv e-prints, arXiv:2111.03634.
<https://arxiv.org/abs/2111.03634>
- Troja, E., Ryan, G., Piro, L., et al. 2018, *Nature Communications*, 9, 4089,
doi: [10.1038/s41467-018-06558-7](https://doi.org/10.1038/s41467-018-06558-7)
- Troja, E., van Eerten, H., Zhang, B., et al. 2020, *Monthly Notices of the Royal Astronomical Society*, 498, 5643,
doi: [10.1093/mnras/staa2626](https://doi.org/10.1093/mnras/staa2626)
- Virgili, F. J., Zhang, B., O'Brien, P., & Troja, E. 2011, *The Astrophysical Journal*, 727, 109,
doi: [10.1088/0004-637x/727/2/109](https://doi.org/10.1088/0004-637x/727/2/109)
- von Kienlin, A., Meegan, C. A., Paciesas, W. S., et al. 2014, *The Astrophysical Journal Supplement Series*, 211, 13,
doi: [10.1088/0067-0049/211/1/13](https://doi.org/10.1088/0067-0049/211/1/13)
- . 2020, *The Astrophysical Journal*, 893, 46,
doi: [10.3847/1538-4357/ab7a18](https://doi.org/10.3847/1538-4357/ab7a18)
- Williams, D., Clark, J. A., Williamson, A. R., & Heng, I. S. 2018, *The Astrophysical Journal*, 858, 79,
doi: [10.3847/1538-4357/aab847](https://doi.org/10.3847/1538-4357/aab847)